Applied Geochemistry 97 (2018) 19–31

Contents lists available at ScienceDirect

Applied Geochemistry

journal homepage: www.elsevier.com/locate/apgeochem

Alteration of synthetic basaltic glass in silica saturated conditions: Analogy with nuclear glass

T. Ducasse[a], A. Gourgiotis[b], E. Pringle[c,d], F. Moynier[c], P. Frugier[a], P. Jollivet[a], S. Gin[a,*]

[a] CEA, DEN, DE2D/SEVT Marcoule, F30207, Bagnols sur Cèze, France
[b] Institut de Radioprotection et de Sûreté Nucléaire (IRSN), PSE-ENV/SEDRE/LELI, Fontenay-aux-Roses, France
[c] Institut de Physique du Globe de Paris, University Paris Diderot, CNRS UMR 7154, Paris, 75005, France
[d] Scripps Institution of Oceanography, UC San Diego, USA

ARTICLE INFO

Editorial handling by Dr D. Wolff-Boenisch

Keywords:
Nuclear glass
Basaltic glass
ISG
Dissolution
Alteration

ABSTRACT

This study investigates the analogy between basaltic and borosilicate glasses of nuclear interest, by focusing on mechanisms controlling glass dissolution under silica saturation conditions. These conditions are representative of a non- or slowly renewed contacting solution, favouring the formation of a potentially passivating silica rich gel layer and secondary phases. Laboratory batch experiments were performed with synthetic basaltic glass altered at 90 °C, at pH 7 in a saturated ^{29}Si-doped aqueous solution for more than 600 days. Using elemental and isotopic solution analysis and solid characterizations by SEM, TEM and ToF-SIMS, we show that basaltic glass corrodes at an unexpectedly high and constant dissolution rate of 4×10^{-3} g m^{-2} d^{-1} associated with the absence of passivating gel. Our results highlight the fact that the dissolution rate is controlled by the hydrolysis of the glassy network, sustained by the precipitation of clay-type minerals and amorphous silica. When tested in similar conditions, the International Simple Glass (ISG), a six oxide borosilicate glasses of nuclear interest displays a much lower rate limited by water diffusion through a passivating layer. The different behavior of the two glasses is explained by their ability to form secondary crystalline phases at the expense of an amorphous passivating film.

1. Introduction

Understanding the processes responsible for the alteration of basaltic glass is of great interest in many research fields. Because of its widespread presence on the ocean floor and in volcanic rock, basaltic glass partly controls the chemical mass balance of the ocean (Benzerara et al., 2007; Morin et al., 2015) and the stability of volcanic terrain (Barone et al., 2016). The geological storage of CO_2 in mafic formations such as basalt bedrock also requires good knowledge of the interactions between water and silicate rock (Gislason et al., 2013; Guyot et al., 2011; Wolff-Boenisch et al., 2011). Studying the alteration of basaltic glass is also important for its use as a natural analogue of nuclear glass to assess the safety of deep geological nuclear waste storage (Crovisier et al., 2003; Ewing, 1979; Libourel et al., 2011; Poinssot and Gin, 2012). The basic idea is that the long-term behavior of nuclear glass can be predicted by a kinetic model provided that this model captures the main processes governing both the short- and long-term behavior of natural glasses.

Considerable experimental work has already been carried out on the first stages of the alteration of basaltic glass (Berger et al., 1987; Crovisier, 1989; Crovisier et al., 1987; Gislason and Eugster, 1987; Gislason and Oelkers, 2003; Techer et al., 2001; Verney-Carron et al., 2011; Wolff-Boenisch et al., 2004) and the nature of the products formed (Jercinovic et al., 1990; Le Gal, 1999; Stockmann et al., 2011). However, the dissolution rate of both borosilicate and aluminosilicate glasses in confined media is known to achieve low values of typically several orders of magnitude lower than the initial dissolution rate (Gin et al., 2012; Parruzot et al., 2015). In these conditions, the silica concentration reaches apparent saturation and the glass dissolves in a steady-state regime also called the residual rate regime (Parruzot et al., 2015; Vienna et al., 2013). Unfortunately, there are too few kinetic measurements and comparisons between in-lab and in-field data to give credit to long-term predictions from existing kinetic models (Daux et al., 1997; Frugier et al., 2008; Grambow and Muller, 2001; Oelkers, 2001).

Parruzot et al. (2015) provided new insights into the long-term alteration in confined media of basaltic glass. These authors measured the residual rates of synthetic basaltic glass in batch experiments at 30 °C

* Corresponding author.
E-mail address: stephane.gin@cea.fr (S. Gin).

https://doi.org/10.1016/j.apgeochem.2018.08.001
Received 27 March 2018; Received in revised form 26 July 2018; Accepted 1 August 2018
Available online 02 August 2018
0883-2927/

and 90 °C and the diffusion coefficient of water and alkali metals from the pristine glass to the solution through the alteration layer. After extrapolating these rates to environmental conditions, Parruzot et al. (2015) showed that the constant residual rates derived from laboratory measurements were in reasonable agreement with the mean apparent rates calculated for natural samples of various ages (Parruzot, 2014). Unfortunately, this approach did not rely on the understanding of the rate-limiting processes assumed to govern the long-term alteration rate of basaltic glasses in nature.

The resistance of glass to aqueous corrosion is not an intrinsic property of the glass but a response to a range of environmental factors. The reactions between silicate glass and water include: (1) the hydration of the glass and ion-exchange between ionic species in water (particularly H^+) and ionic components in the glass (primarily alkali) (2) the hydrolysis of network forming species (e.g., Si, B, Al); and (3) the transport of hydrolyzed species into the solution. As these three primary reactions proceed, glass components are released into the solution and/or are incorporated into alteration products (amorphous and crystalline phases) on the surface of the reacting glass. The reaction rates are controlled by many factors, chief among which are the glass composition, the temperature and pH of the solution and the concentration of the species dissolved in the solution (e.g., H_4SiO_4 and $Al(OH)_4^-$). These processes have been summarized in many reviews (Bunker, 1994; Fournier et al., 2014; Gin, 2014; Gin et al., 2013a; Inagaki et al., 1998; Jantzen et al., 2010; Van Iseghem et al., 2006, 2009; Vienna et al., 2013).

The amorphous phase formed on the surface of the glass by the hydrolysis and condensation of glass forming species can be transport-limiting in some situations (Cailleteau et al., 2008, 2011; Gin et al., 2015a; Jollivet et al., 2008; Rebiscoul et al., 2004, 2005). The mechanism responsible for the formation of this so called “passivating layer” is currently the subject of debate. Observations of sharp interfacial gradients have led some authors to propose that the glass dissolves congruently within a thin interfacial film of water. The alteration products then form by precipitation from species released in this film (Geisler et al., 2010, 2015; Hellmann et al., 2015; Putnis, 2015). This interpretation has been supported by isotope studies: the altered layer of a silicate sample was shown to be enriched in isotopes such as ^{18}O and ^{26}Mg artificially introduced into the contacted solution, with no observable sigmoid diffusion profile (Geisler et al., 2015).

More recently, Gin et al. (2016) replicated a key experiment of Hellmann et al. (2015) and concluded that processes by which the passivating gel forms is dependent on both the glass composition and the leaching conditions. An alternative model has been proposed on the basis of experiments conducted with International Simple Glass (ISG), a six-oxide borosilicate glass. In near-neutral and slightly alkaline pH conditions, the passivating film in this model forms a low diffusive structure by in-situ reorganization of the silicate network after the release of the most soluble species (Na, B, Ca). The reorganization of the silicate network would explain the lower water diffusion coefficients in this layer than in the pristine glass (Gin et al., 2015a, 2017, 2018).

The present study aims at determining whether the processes described for nuclear glasses also occur during the alteration of basaltic glass. Using a multi-scale approach including the characterization of both liquids and solids, we investigate the processes governing alteration of basaltic glass in steady-state conditions. In this article we report the results of experiments conducted using the same protocol as the one used for ISG (Gin et al., 2015a): a long-term static test was performed over 600 days with glass powder and coupons placed in contact with water initially saturated with respect to SiO_2(am) at 90 °C and $pH_{90°C}$ 7. Our results show that there are major differences between the two glasses and highlight that the precipitation of secondary crystalline or amorphous phases dominates over the formation of a passivating film.

2. Material and methods

2.1. Reagents and samples

All the solution aliquots were diluted with 0.5 M nitric acid obtained from distillated 15 M ($mol\,L^{-1}$) nitric acid (EVAPOCLEAN system, Analab, France) and 18 MΩ cm de-ionized water (Milli Q system, Millipore, Milford, MA, USA).

2.2. Glass preparation

A model basaltic glass (BG_B) was prepared and doped with the equivalent of 1 wt% B_2O_3 as a potential alteration tracer. Since boron is not present in natural basaltic glasses, a small amount of B_2O_3 has been chosen to remain as representative of natural materials as possible. The composition of BG_B is similar to that of the glass synthetized by Techer and coworkers (Techer et al., 2000). The precursors were oxide, carbonate, oxalate and nitrate powders. After weighing, the powders were poured into a Pt-Rh crucible. Two melts were prepared at 1500 °C in an electric furnace with 3 h of refining. Part of the glass was quenched; the remainder was cast into a graphite mold and annealed at 700 °C for 3 h in an electric oven and cooled to room temperature.

From the resulting glass bars, eight monoliths of 1 × 1 × 0.1 cm^3 each were prepared. The two large faces were polished up to grade 4000 using SiC paper. The density measured for these samples from the glass bar on a hydrostatic balance was 2.793 ± 0.0005 $g\,cm^{-3}$ (Parruzot et al., 2015).

Quenched BG_B glass samples were ground and milled to obtain a mean particle diameter between 125 and 200 µm. Fine particles were removed by washing the glass powder in absolute ethanol several times and allowing the powder to settle at appropriate times calculated using Stokes' law. The specific surface area of the powder was measured at 0.0295 ± 0.0015 $m^2\,g^{-1}$ by krypton absorption using the Brunauer, Emett and Teller (BET) method (Brunauer et al., 1938). Laser diffraction (Malvern Mastersizer 3000) was used to calculate the particle size distribution and geometric surface area from the measured angular variation in the scattered light intensity produced by a laser beam passing through a dispersed particulate sample. As glass grains are not spherical but rather ellipsoidal, we used the technique described by (Fournier et al., 2016) to determine the size fraction. The angular scattering intensity data were analyzed to calculate the size of the particles responsible for the scattering pattern, using Mie theory and a volume equivalent sphere model. The refractive indices were taken to be 1.54 for the glass and 1.33 for the dispersant (water). The results were divided into 100 size fractions logarithmically distributed between 10^{-2} and $3{\cdot}10^3$ µm. The BG_B 125–200 µm powder had a particle size distribution centered on 160 µm and a geometric surface area of 0.0125 $m^2\,g^{-1}$, leading to a ratio between the BET and the geometric surface area of 2.36, which is common for glass particles (Fournier et al., 2016; Icenhower and Steefel, 2015).

Elemental concentrations in the glass were determined by Inductively Coupled Plasma Optical Emission Spectroscopy (ICP-OES) after dissolution of the glass by alkaline fusion followed by neutralization with HNO_3 (Table 1). A similar protocol was used to dissolve $^{29}SiO_2$ (see below and (Gin et al., 2015b)). The concentration uncertainties were estimated to be ± 5% for elements with more than 1 wt % in the glass, and ± 10% for less concentrated elements. An uncertainty of ± 25% was considered for B concentrations which were close to the detection limit.

2.3. Leaching experiments

2.3.1. Main leaching experiment

The main leaching experiment involved studying the alteration of both 8 coupons (~19 cm^2 based on geometric considerations) and 0.38 g of 125–200 µm BG_B glass powder (~112 cm^2 based on BET

Table 1
Glass composition (wt%). Uncertainties are given in brackets. Glass CJ1 (Jegou et al., 2000) and international simple glass (ISG) (Gin et al., 2013a) are considered in this study for comparison.

BG_B	SiO_2	Al_2O_3	Fe_2O_3	CaO	MgO	Na_2O	TiO_2	B_2O_3	SrO	K_2O	MnO_2	P_2O_5	ZrO_2
ISG	54.1(2.7)	15.9(0.8)	9.6(0.5)	8.1(0.4)	5.8(0.3)	2.6(0.1)	1.5(0.1)	1.0(0.1)	0.5(0.05)	0.2(0.02)	0.4(0.04)	0.3(0.03)	–
	56.2(2.8)	6.1(0.3)	–	5.0(0.3)	–	12.2(0.6)	–	17.3(0.9)	–	–	–	–	3.3(0.2)
CJ1	68.1(3.4)					10.9(0.5)		21.0(1.0)					

measurement) at 90 °C in static mode, placed in 140 mL of solution leading to a low glass-surface area-to-leaching-solution-volume ratio (S/V, m^{-1}) of ~60 m^{-1}. Coupons are placed in Teflon baskets so that they are not in direct contact with the glass powder. The solution was initially enriched with ^{29}Si up to a concentration close to the saturation with respect to amorphous silica. The perfluoroalkoxy (PFA) vessel with the glass and the leachate was packed into a container with a few milliliters of water to minimize evaporation in the reactor. The double container was then stored in an oven at 90 °C (± 1 °C) for the duration of the experiments. The $pH_{90°C}$ of the leachate was initially adjusted to 7.0 (± 0.2); regularly monitored at 90 °C and maintained at this value until the end of the experiment by adding small amounts of 0.5 mol L^{-1} HNO_3 (Suprapur) or 0.5 mol L^{-1} NaOH (PROLABO, NORMADOSE). At different times, the leachate was sampled and a coupon was withdrawn for characterization.

The leaching solution was prepared as follows. $^{29}SiO_2$ (Eurisotop, ^{29}Si > 95%) was mixed with KOH (Suprapur) and melted at 600 °C. The resulting potassium silicate was dissolved in deionized water at 90 °C to obtain a Si concentration of 160 mg L^{-1} at $pH_{90°C}$ 7. The resulting $^{29}Si/^{28}Si$ ratio in the solution was 28.9, compared with 0.0507 in the glass (natural abundance). This protocol yielded a K concentration in the onset solution of 2.5 g L^{-1}. Note that a previous work on ISG demonstrated that K significantly affects the glass dissolution rate in silica saturated conditions (Collin et al., 2018). In order to compare the behavior of basaltic glass and ISG, it was decided to conduct the experiment in similar conditions.

One glass coupon was withdrawn, rinsed with deionized water and dried for 2 h at 90 °C for characterization after 1, 14, 91, 210, 365 and 600 days. In parallel, 0.5 mL samples of the liquid were taken from the reactor during the experiment, diluted and acidified with 2.5 mL of 0.5 mol L^{-1} HNO_3 (Suprapur), and filtered at 0.45 µm before analysis. Note that the aliquots were diluted with 0.5 N HNO_3 prior to filtration to prevent silica precipitation as the solution was cooled. At each sampling time, the pH was recorded at 90 °C. The leaching solution was not topped up during the experiment so the volume change in the reactor was taken into account in calculations of the normalized mass losses of the glass. Possible evaporation between sampling times was also taken into account by weighing the reactor before and after each sampling.

2.3.2. Complementary leaching experiment

Because the concentration of the glass dissolution tracers was difficult to measure in the solution of the main leaching experiment, a second experiment with a higher S/V ratio was performed under the same conditions. This test was conducted with the same glass, in a solution at a fixed $pH_{90°C}$ of 7 saturated with respect to amorphous silica (at natural isotopic abundance). The S/V ratio of 20000 m^{-1} was obtained by placing 0.6557 g of BG_B powder (crushed, sieved, and ultrasonically cleaned; BET specific surface area, 2.318 m^2 g^{-1}) in contact with 80 mL of leaching solution. The leachate was regularly sampled and the aliquots were analyzed by ICP-OES.

2.4. Solution analysis

The leaching solution samples were analyzed by ICP-OES (ThermoScientific ICAP 6300 DUO) after dilution and acidification with HNO_3. The uncertainties on the concentrations obtained are 3% for Si, Al, Ca, Fe, Mg and Na, and 50% for B due to its low concentration. For the complementary tests performed at an S/V ratio of 20000 m^{-1}, the Si and B concentrations were measured separately by spectrophotometry (Merck Spectroquant TEST, Cary 50 Scan UV–Vis spectrophotometer). The boron concentration in the samples taken at 400, 610 and 700 days in the main experiment was measured by Inductively Coupled Plasma – Mass Spectrometry (ICP-MS, Thermofisher Scientific ICAPQ).

Because B is known to be a good tracer of glass dissolution (i.e., it does not precipitate and it is not retained in the alteration products), the equivalent thickness of altered glass, *Eth,* was calculated from the B concentration at a given sampling time, taking into account the particle size decrease, as follow:

$$ETh(\mathrm{B})_t = ETh(\mathrm{B})_{t-1} + \frac{(C(\mathrm{B})_t - C(\mathrm{B})_{t-1})V_t}{\rho \times S_t \times x_\mathrm{B}} \quad (1)$$

Where *Eth* in m, *C(B)* is the B concentration in $g.L^{-1}$, V_t the volume in L of the solution at time *t*, ρ the density of the glass (2.793×10^6 g m^{-3}), S_t the reactive surface area in m at time *t*, and x_B the mass fraction of B in the glass.

$$r = \frac{ETh(\mathrm{B}) \times \rho}{t} \quad (2)$$

With *ETh*(B) in meters, ρ in $g.m^{-3}$ and t in days. As a first approximation, the glass dissolution rate at time *t* was calculated by linear regression on three points from t_{-1} to t_{+1}. Based on the analytical errors on ICP data and on the determination of glass surface, the estimation of the relative uncertainties for *ETh* and *r* are 30%.

2.5. Silicon isotope analysis

Prior to silicon isotope analysis, all samples and standards were purified using BioRad AG50 X-12 (200–400 mesh) cation exchange resin, following the method used in FM's laboratory at the Institut de Physique du Globe de Paris (Pringle et al., 2014, 2016; Savage and Moynier, 2013) adapted from a previous work (Georg et al., 2006).

For the samples taken until 203 days into the experiment, the silicon isotope ratio measurements were performed on a Thermo Scientific Neptune Plus Multi-Collector Inductively Coupled Plasma Mass-Spectrometer (MC-ICPMS) housed in Paris, France at the Institut de Physique du Globe de Paris. The instrument was operated at medium resolution to avoid Si polyatomic interferences following the same method as in Pringle et al. (2014, 2016).

For the samples taken later than 203 days into the experiment, the silicon isotope ratio measurements were performed on an Agilent 8800 tandem quadrupole ICP-MS/MS instrument, at the Institut de Radioprotection et de Sûreté Nucléaire (IRSN, Fontenay-aux-Roses, France).

According to the method described in detail in (Gourgiotis et al., 2017), silicon isotope ratio determination is performed in mass-shift mode using SiO_2^+ ion species to avoid Si polyatomic interferences. ICP-MS/MS is a simple and low cost technique compared to the MC-ICPMS, providing Si isotope ratios with uncertainties of ~0.5% which meet the

Table 2
Solution analysis results. The B concentrations followed by a* symbol were measured by ICP-MS. The concentrations of the different silicon isotopes were measured by MC-ICP-MS for experiment times up to 203 days and by ICP-MS/MS thereafter. Day 0 corresponds to the onset solution.

t (days)	$pH_{90°C}$	Si_{tot}	$^{29}Si/^{28}Si$	$^{30}Si/^{28}Si$	^{28}Si	^{29}Si	^{30}Si	B	Na	Al	Ca	Fe	Mg
		($mg.L^{-1}$)	wt%	wt%	($mg.L^{-1}$)	($mg.L^{-1}$)	($mg.L^{-1}$)	($mg.L^{-1}$)	($mg.L^{-1}$)	($mg.L^{-1}$)	($mg.L^{-1}$)	($mg.L^{-1}$)	($mg.L^{-1}$)
0	7.0	160.0	n.d.	n.d.	5.1	151.2	3.7	< 0.3	5.6	< 0.3	2.6	< 0.3	< 0.3
1	7.1	165.6	8.403	0.038	17.0	147.9	0.7	< 0.3	3.8	< 0.3	2.8	< 0.3	< 0.3
3	7.2	156.9	8.161	0.038	16.5	139.7	0.7	< 0.3	3.5	< 0.3	2.6	< 0.3	< 0.3
7	7.0	157.9	8.052	0.038	16.8	140.4	0.7	< 0.3	2.9	< 0.3	2.7	< 0.3	< 0.3
14	7.1	166.6	7.527	0.038	18.8	146.9	0.7	< 0.3	2.9	< 0.3	2.8	< 0.3	< 0.3
28	7.1	167.5	7,75	0.038	18.5	148.2	0.7	< 0.3	4.4	< 0.3	4.7	< 0.3	< 0.3
62	7.1	164.2	7.100	0.038	19.6	143.8	0.8	< 0.3	2.8	< 0.3	2.6	< 0.3	0.4
91	7.0	168.1	6.619	0.038	21.3	145.9	0.8	< 0.3	3.9	1.4	3.5	2.1	0.5
171	7.0	176.1	5.453	0.037	26.3	148.7	1.0	< 0.3	2.8	0.8	3.3	1.4	0.6
203	7.0	150.9	5.162	0.036	23.6	126.3	0.9	< 0.3	5.7	0.8	4.2	0.8	0.7
273	6.8	177.2	4.715	0.036	29.9	146.1	1.1	< 0.3	9.4	< 0.3	4.0	< 0.3	0.6
362	7.0	181.2	4.235	0.036	33.4	146.5	1.3	< 0.3	6.8	< 0.3	2.8	< 0.3	0.4
400	7.1	–			–	–	–	0.12*	–	–	–	–	–
562	7.0	183.7	3.175	0.035	42.5	139.6	1.6	< 0.3	5.6	< 0.3	3.2	< 0.3	< 0.3
610	7.0	194.9			–	–	–	0.13*	9.9	< 0.3	2.9	< 0.3	0.5
700	7.0	226.4			–	–	–	0.18*	7.7	< 0.3	6.3	< 0.3	0.3

requirements for nuclear glasses studies.

The weight percentage of each isotope was calculated for each sample using the isotope ratios (Table 2) according the following equation:

$$\%weight\ ^{x}\mathrm{S\ i} = \frac{\frac{M_{Si^x}}{M_{Si^{28}}}\left(\frac{^{x}Si}{^{28}Si}\right)_{atomic}}{\sum_{x=28}^{30}\left[\frac{M_{Si^x}}{M_{Si^{28}}}\left(\frac{^{x}Si}{^{28}Si}\right)_{atomic}\right]} \quad (3)$$

With M_{Si^x}, the molar mass of Si isotope x (x = 28, 29 or 30).

Then, the concentration of each isotope in solution was determined using the next equation:

$$[^{x}Si] = \%weight\ ^{x}\mathrm{S\ i} \times [Si]_{tot} \quad (4)$$

Where $[Si]_{tot}$, is the total Si concentration measured by ICP-OES. The results can be found in Table 2.

2.6. Solid characterizations

The morphology of the samples of altered glass powder was characterized by Scanning Electron Microscopy (SEM) using a Zeiss Gemini Supra 55 FEG-SEM system operated at an acceleration voltage of 15 kV.

A Time-of-Flight Secondary Ion Mass Spectrometer (ToF-SIMS) (TOF.SIMS5, IONTOF GmbH, Münster, Germany) was used to perform elemental and isotopic depth profiling analyses. Two sputtering beams abrading a surface area of 350 × 350 μm^2 were used: a 500 eV 40 nA Cs^+ beam when analyzing anions and a 500 eV 100 nA O_2^+ beam when analyzing cations. The beam energy was limited to 500 eV to obtain more accurate data on the external part of the alteration layer. The anions and cations were analyzed using a Bi^+ 25 keV ion beam at 2 pA over an area measuring 100 × 100 μm^2. The surface charges created during the analysis were neutralized using a pulsed low-energy (< 20 eV) electron flux.

Parts of the coupon and powder sample altered for 600 days were embedded in epoxy resin, polished to a mirror finished and characterized by Transmission Electron Microscopy (TEM). Focused ion beam (FIB) milling was performed with a FEI 200 dual beam FIB system at the University of Aix-Marseille, (Marseille, France). The FIB lamella was prepared with a 30 kV Ga^+ beam operating at ~20 nA. The prepared lamella measuring approximately 12 × 5 × 0.1 μm^3 was transferred at atmospheric pressure with a micromanipulator to the membrane of a carbon-coated 200 mesh copper grid prior to TEM observations. Morphological observations and Energy-Dispersive X-ray (EDX) analyses were carried out on a Technai G2 (FEI) TEM instrument equipped with a LaB_6 source operating at 200 kV. The detectors were a Gatan CCD camera, a STEM BF-DF detector, and an EDAX Genesis for the EDX analyses. The EDX probe size was 5 nm. The EDX analyses were performed in STEM mode on large windows of 100 nm^2 to minimize the volatilization of light elements such as sodium.

3. Results

3.1. Solution analysis

Table 2 shows the concentrations of the major elements in the samples taken during the main experiment and the pH of the leaching solution measured just before each sample was taken. The pH remains within the target range throughout the experiment.

The total silicon concentration as a function of time, plotted in Fig. 1, increases slowly in spite of the high initial concentration, to reach more than 200 mg L^{-1} at the end of the experiment. This level corresponds to the saturation with respect to amorphous silica. Note that in long-term leaching tests conducted in initially pure water on simplified nuclear glasses including ISG, silica concentration increases over time toward saturation with respect to amorphous silica (Gin et al., 2012). However, our result may appear surprising given that Parruzzot et al. (2015), starting with deionized water found a silica saturation concentration much lower than the saturation level with respect to amorphous silica in their residual rate experiments on basaltic glass. The hypothesis that the saturation the solution with respect to SiO_2 stops the hydrolysis of the glass network, which was verified for ISG (Gin et al., 2015a, 2017), is called into question by this result. The behavior of the silicon isotopes will clarify this point.

The concentrations of Al, Fe and B are below the ICP-OES quantification limit. The B concentrations were measured at three sampling times by ICP-MS but carry a large uncertainty (≥50%) because of the low available quantities for precise measurement. The Na concentrations cannot be interpreted because of contamination from the HNO_3 added regularly to maintain the pH at 7. Indeed, commercial nitric acid (Suprapur) contains traces of Na and the amount of Na released by the glass is so small that contamination with HNO_3 prevents the exploitation of the measured Na concentrations.

3.2. Solid characterization

3.2.1. Scanning electron microscopy

Glass powder altered for 700 days and a monolith altered for 600 days were observed by SEM and compared to pristine glass (Fig. 2). The

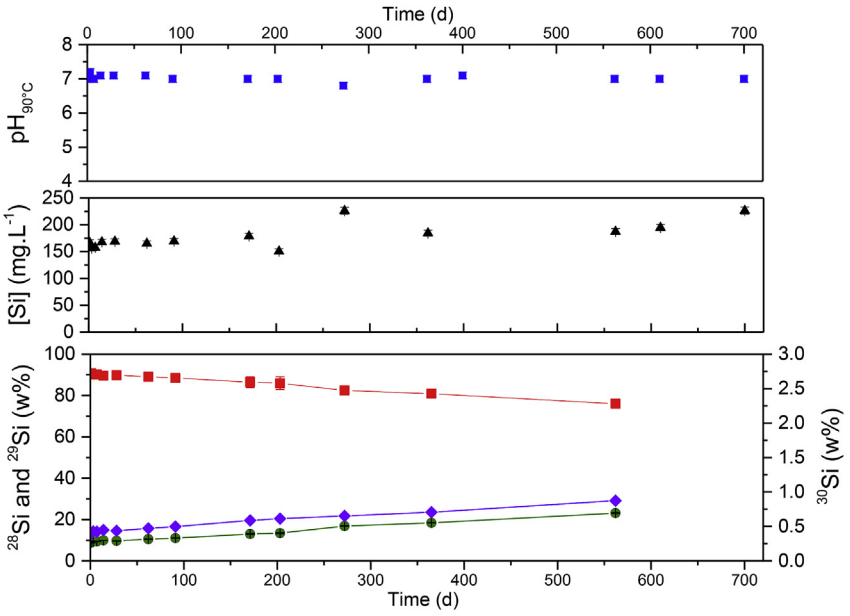

Fig. 1. Top: pH measured at 90 °C (■); middle: Total Si concentration (▲), and bottom: relative weight percentages of ^{28}Si (◆), ^{29}Si(■) and ^{30}Si(●) as a function of time.

surface of the polished monolith (Fig. 2a) is much smoother than that of the grains of pristine glass obtained by crushing. No alteration layer was observed at SEM resolution (~100 nm) on the surface of the monolith (Fig. 2c and d) or of the altered glass (Fig. 2e and f), whereas the thickness of the alteration layer calculated from the solution data ranges from 360 to 750 nm (Fig. 7). This suggests that the glass dissolves congruently, with no gel formation replacing the altered glass as it is the case for ISG in similar conditions (Gin et al., 2015a).

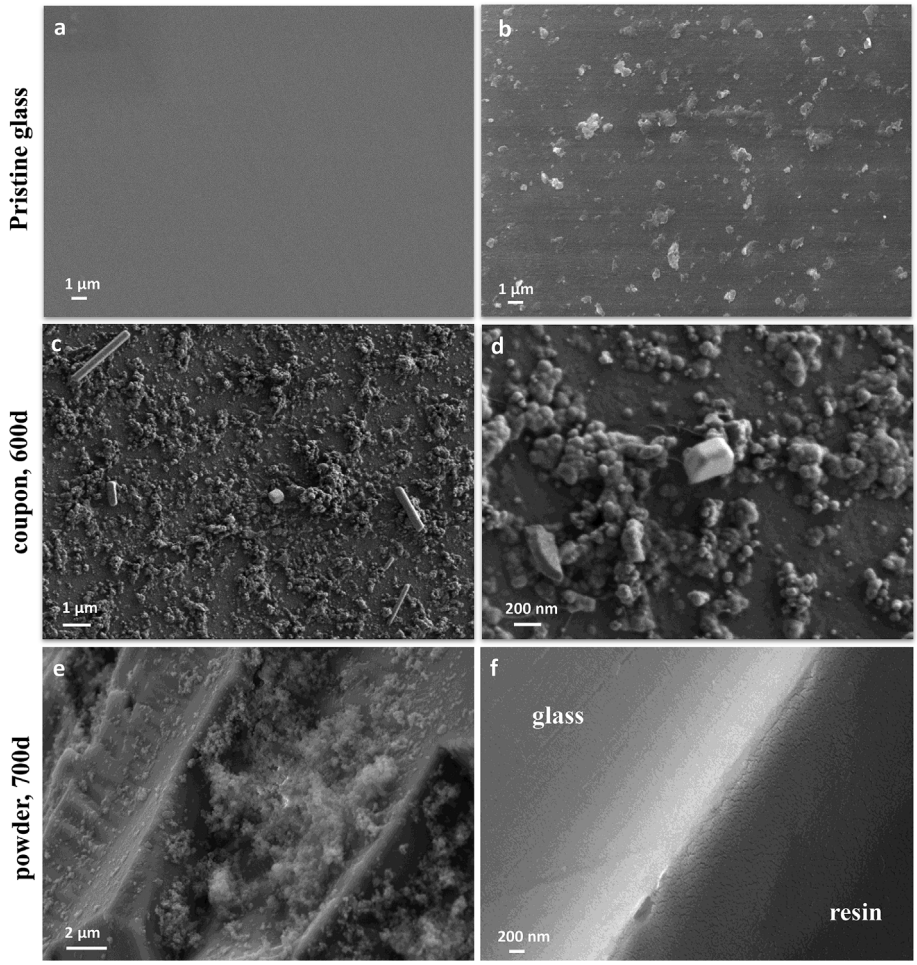

Fig. 2. Scanning electron micrographs (back-scattered electrons) of BG_B glass: a) a pristine coupon, b) a pristine grain, c) and d) the surface of a coupon altered for 600 days, e) the surface of a grain altered for 700 days, and f) the cross-section of a representative grain altered for 700 days.

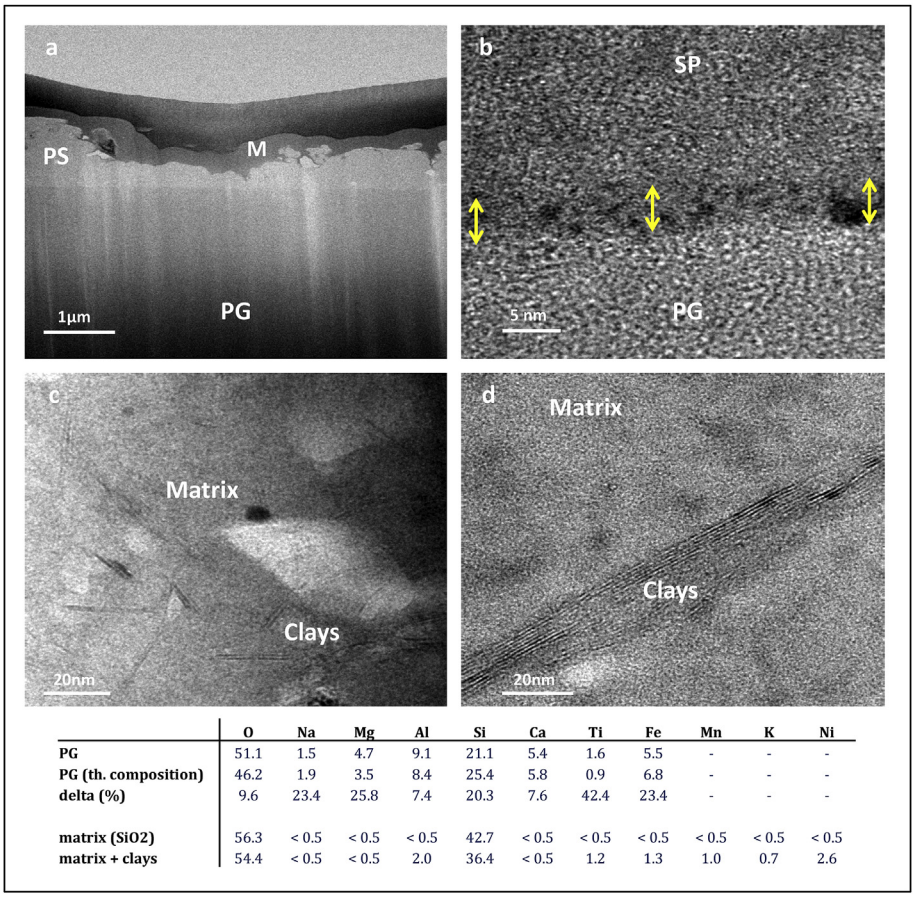

	O	Na	Mg	Al	Si	Ca	Ti	Fe	Mn	K	Ni
PG	51.1	1.5	4.7	9.1	21.1	5.4	1.6	5.5	-	-	-
PG (th. composition)	46.2	1.9	3.5	8.4	25.4	5.8	0.9	6.8	-	-	-
delta (%)	9.6	23.4	25.8	7.4	20.3	7.6	42.4	23.4	-	-	-
matrix (SiO_2)	56.3	< 0.5	< 0.5	< 0.5	42.7	< 0.5	< 0.5	< 0.5	< 0.5	< 0.5	< 0.5
matrix + clays	54.4	< 0.5	< 0.5	2.0	36.4	< 0.5	1.2	1.3	1.0	0.7	2.6

Fig. 3. STEM images of the monolith of BG_B glass altered for 600 days. a) the entire cross section (with the metallization layer, M), b) the interface between the pristine glass (PG) and the secondary phases (SP), and c) and d) the secondary phases. The yellow arrows in part b) delimit the reactive interface. The table gives the results of a semi-quantitative EDX analysis of the different compounds (wt%). A comparison between the analyzed PG and the nominal composition indicates the analytical error (delta). (For interpretation of the references to colour in this figure legend, the reader is referred to the Web version of this article.)

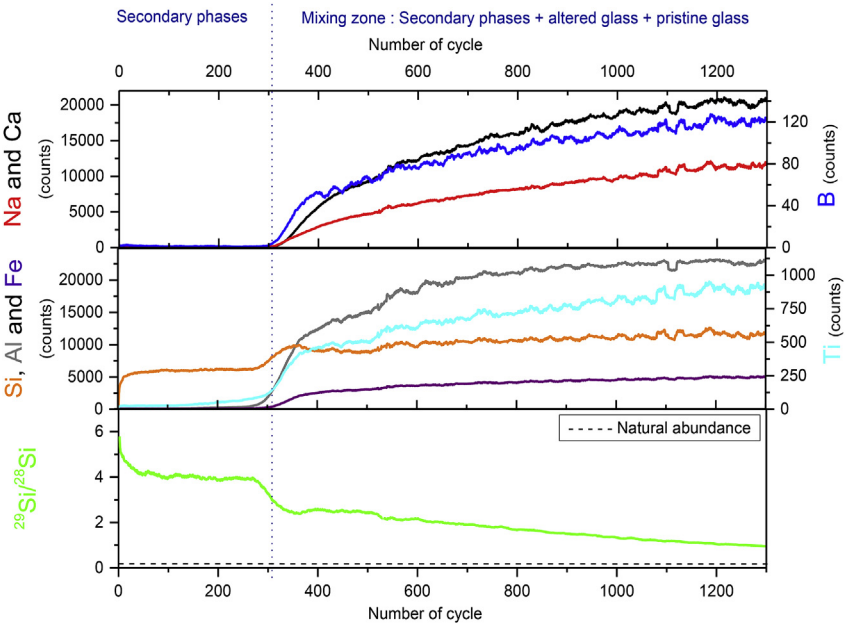

Fig. 4. Tof-SIMS depth profiling of BG_B glass altered 600 days. Because of the roughness of the outer surface which affects the location of the interfaces, data are plotted in cycles rather than in nm. Top: Unnormalized Na, Ca and B elemental profiles. Middle: Unnormalized Si, Al, Fe and Ti elemental profiles. Bottom: quantitative $^{29}Si/^{28}Si$ isotopic ratio.

The micrographs show that different secondary phases form on the glass surface during alteration (Fig. 2c, d and e): a few sparsely spread crystals and more or less spherical phases. The amounts formed on the glass surface are too small for chemical (EDX) or structural (X-ray diffraction) analysis. The spherules observed here resemble the amorphous silica particles observed during the dissolution of CJ1 ternary borosilicate glass (Jégou et al., 2000).

3.2.2. *Transmission Electron Microscopy*

The monolith altered for 600 days was observed by TEM. Fig. 3 shows an overall view of the sample prepared by focused ion beam (FIB) thinning. The glass is covered by a very uneven layer of certainly precipitated secondary phases (SP). The morphology of the particles making up this layer, which is between 100 nm and 1 µm thick, matches that of the phases observed by SEM (Fig. 2 c, d and e). At this resolution, as in the SEM images (Fig. 2f), there is no sign of any gel or

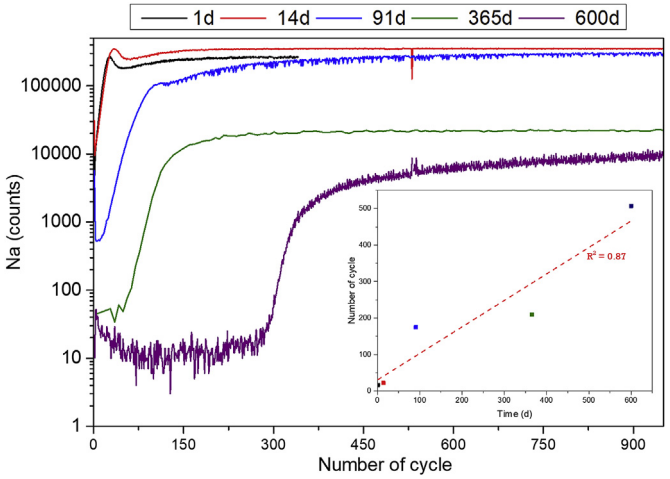

Fig. 5. Unnormalized Na profiles recorded for glass monoliths altered for 1, 14, 91, 365 and 600 days. Inset: evolution of the Na sharp gradient (taken at the half height) as a function of the number of abrasion/analysis cycles.

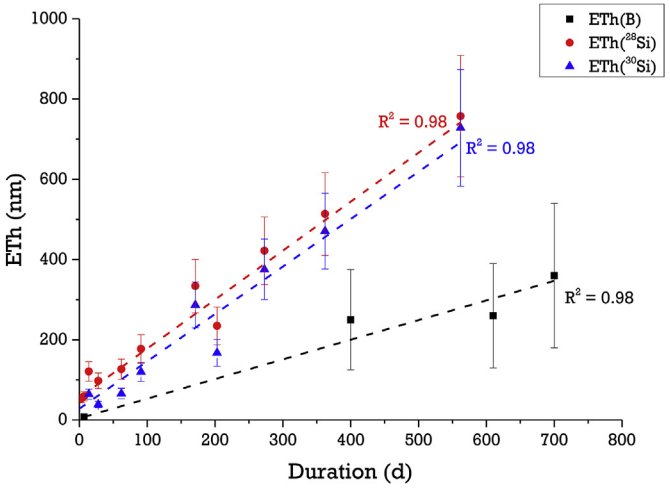

Fig. 6. Comparison of the evolution versus time of ETh calculated from B, ^{28}Si and ^{30}Si release in solution.

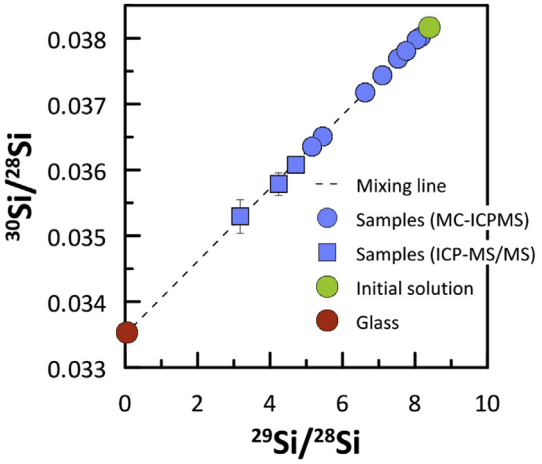

Fig. 7. ^{30}Si/^{28}Si isotope ratio as a function of the ^{29}Si/^{28}Si ratio, showing a binary mixing between two endmembers: the solution at the start of the experiment, enriched in ^{29}Si (green dot), and the natural abundance of Si (red dot). It can be noted the two analytical techniques used in this study provide the same trend. (For interpretation of the references to colour in this figure legend, the reader is referred to the Web version of this article.)

hydrated glass layer between the pristine glass and the precipitated phases. A high-resolution analysis of the interfacial region (Fig. 3b) reveals a 5 nm thick layer morphologically different from that of the pristine glass, which could be the reactive interface (in yellow in the figure). This region may therefore be where the hydrolysis reactions occur in this material. The layer is too thin for in-depth characterization however and the EDX profiles reveal nothing of significance (data not shown).

The images of the precipitated phases in parts c and d of Fig. 3 show that they consist of crystalline clay-type phases within an amorphous (mainly amorphous silica) matrix. The chemical composition of these phases is given in the table displayed in Fig. 3. The values are only qualitative. The corresponding uncertainties can be estimated from the difference between the EDX-measured composition of the pristine glass and its theoretical composition. The small size of the clay particles combined with the need to perform the EDX analyses over large areas to avoid any volatilization of light elements such as Na made it impossible to measure the composition of the clay particles alone. This analysis thus provides just a comparison of regions containing secondary phases (matrix + clays) with those that do not (matrix alone). These measurements show primarily that the matrix in which the clays form consists mainly of amorphous silica. The areas containing clay particles are enriched in Mg, Al, K, Ti, Mn, Fe and Ni. The latter, of which there are only trace amounts in BG_B, is present in the initial solution from the Ni crucible used to incorporate ^{29}Si by alkaline fusion. The fact that the clay particles precipitated inside the amorphous silica matrix prevents their identification by X-ray diffraction. Nonetheless the atomic planes of these minerals are clearly visible in Fig. 3 d. The interplanar distance, the distance between two dark or light fringes, is ~10.7 Å. This is the value obtained by taking the average distance between 3 and 8 of the planes shown in Fig. 3 d. Assuming that this distance corresponds to a partly dehydrated structure, the obtained value suggests that the clays could be 2:1 di- or tri-octahedral clays, with an octahedral layer sandwiched between two tetrahedral sheets. The interplanar distance, the approximate composition are all characteristic of smectites, which typically form during the alteration of basaltic glasses (Crovisier et al., 2003). The amount of clay formed is however much lower than reported in the above mentioned study or in Parruzot et al. (2015). This may because the pH affects the growth rate of the clays (Aréna, 2016).

3.2.3. *Time-of-flight secondary ion Mass Spectrometry*

One monolith of pristine glass and monolith samples extracted at 1, 14, 91, 365 and 600 days of alteration were analyzed by ToF-SIMS. The element profiles in the pristine glass were measured in this way to assess the surface state of the glass before alteration. Sample preparation and reactions with the atmosphere only modify the chemical composition of the monolith to a depth of ~5 nm.

The distribution of the major elements in the glass after 600 days of alteration are shown in Fig. 4. These elemental profiles should be interpreted with caution because the high roughness of the precipitate layer creates spurious gradients. This issue is discussed further below. Nonetheless, the profiles for Fe, Al, Ti, B, Na and Ca are clearly similar, with a strong or complete depletion near the outer surface followed by a gradual increase and then a leveling off once the unaltered depth is reached. The silicon profile near the surface shows that the secondary phases contain mostly silicon. These also seem to contain small amounts of aluminum and titanium.

Fig. 4 also presents the isotopic signature of silicon in the alteration layer. The secondary phases display a ^{29}Si/^{28}Si ratio ranging between 3 and 6, which is much higher that the glass signal (0.05). This interval stays within that recorded in the solution (from 10 in the onset solution to 3.5 after 562 days (Table 2)), strongly suggesting that these phases precipitate from aqueous species.

The sodium profiles at different sampling times show how alteration proceeds (Fig. 5). All the profiles, which were measured in the same way, indicate strong surface depletion, then a pseudo-gradient up to a

plateau that marks the boundary with the unaltered material.

4. Discussion

4.1. Alteration kinetics of the basaltic glass

Boron is generally used as glass alteration marker but in our case its concentration was below the quantification limit at most of the measurement times. This is a direct consequence of the low S/V ratio chosen for this study. Recall that this choice was motivated by the need to limit pH variations caused by the release of alkaline and alkaline earth elements from the glass. Sodium can often be used as an alteration marker because it is as soluble as boron and rarely precipitates in secondary phases (Parruzot et al., 2015). This was not possible for this experiment however because most of the sodium present in solution came as a contaminant with HNO_3 used to control the pH. The other elements released from the glass are all liable to be retained in the alteration layer. Boron was therefore deemed to be the best available alteration marker.

The equivalent thicknesses of altered glass calculated from the boron concentration in solution are shown in Fig. 6. The value at 7 days is the one measured in the complementary experiment performed at an S/V ratio of 20000 m^{-1} (cf. appendix 1). This datum can be used assuming that the S/V ratio has no effect on the rate at which the mobile elements in the glass are released under these conditions. This hypothesis, verified for ISG (Gin et al., 2013b), was extended to these conditions. Despite large uncertainties due to the low concentration of B, Fig. 6 suggests that this element could be released linearly over time (R^2 = 0.98); which would be consistent with a constant alteration rate. As B is a glass former, and as activation energy for the hydrolysis of B-O-M (M = Si, Al, Fe, …) bonds is lower than that of Si-O-Si bonds (Zapol et al., 2013), boron release may thus be associated with the dissolution of the silicate network. However, this is not always the case, because, as further discussed, B can be released without a complete dissolution of the silicate network (Gin et al., 2015a, 2018). As a consequence the behavior of Si must be investigated separately.

As can be seen in Fig. 1, silicon isotope concentrations increase with time, with a more pronounced increase for ^{28}Si and ^{30}Si as the solution was initially depleted in these isotopes. This would also suggest that the silicate network dissolves in the tested conditions. This can be evaluated more quantitatively.

In Fig. 7 isotope ratios are represented in a three isotope plot $^{30}Si/^{28}Si$ vs $^{29}Si/^{28}Si$. All data follow a straight line between two end-members, the initial isotope signature of the solution (green dot) and the natural silicon isotope ratio of the glass (red dot). For the initial isotope signature of the solution measured data on day one and Si isotope ratios of the IRMM-018a (Valkiers et al., 2005) for the glass, were respectively used.

This result is a robust proof that the isotopic variations observed in solution are the result of a binary mixing and the mechanism involved must therefore be hydrolysis of the glass leading to the release of silicon into the solution.

The mixing factor for ^{28}Si between the glass and the solution, F, i.e. the proportion of ^{28}Si from the glass in the total amount [^{28}Si in the initial solution + ^{28}Si released from the glass] measured in solution, can be calculated precisely from the relationship describing the isotopic mixing between the two extremes. This is shown in Fig. 8, with the 1-day solution used once more as a reference.

$$Radded_{mixture} = Radded_{glass} * F + (1 - F) * Radded_{solution} \quad (5)$$

Solving this equation for F yields the data for ^{28}Si shown in Fig. 8.

This method is accurate because it only involves isotopic ratios that are precisely measured. The values obtained are in good agreement with the data discussed previously in this section. At 562 days for instance, the calculated mixing factor is 62% and the value obtained from

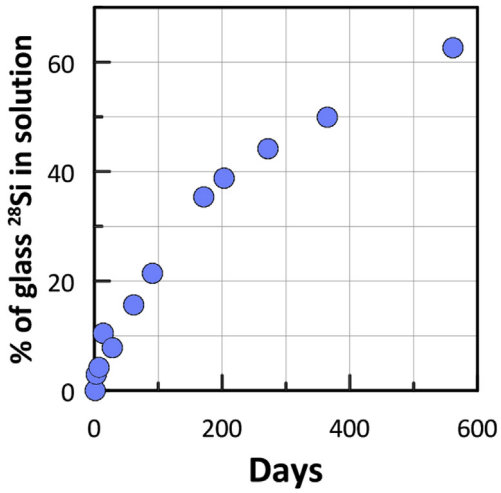

Fig. 8. Evolution over time of the proportion of ^{28}Si released from the glass in the total amount in solution.

Table 2, ($^{28}Si_{562d}$ – $^{28}Si_{1d}$)/$^{28}Si_{562d}$ *100, is 65%.

Overall these isotopic analyses demonstrate that the silicate network of the glass dissolves, releasing orthosilicic acid into the solution, which mixes with that already present, and amorphous silica then precipitates on the glass surface. The amounts of ^{28}Si and ^{30}Si released from the glass can be used to calculate an equivalent thickness of altered glass (Fig. 6). Both isotopes give the same results and show the glass dissolve at a constant rate. However, the equivalent thicknesses calculated from the silicon isotopes are a factor 2 larger than those calculated from the boron concentrations. This difference is surprising and suggests that either the total silicon concentration in the solution was overestimated or that of boron underestimated. This second hypothesis is the most plausible given the large uncertainties associated with the measurements of very low boron concentrations.

The alteration rates calculated for BG_B from the boron, ^{28}Si and ^{30}Si concentrations are respectively (1.9 ± 0.6) $\times 10^{-3}$, (3.9 ± 0.2) $\times 10^{-3}$ and (4.4 ± 0.3) $\times 10^{-3}$ g m^{-2} d^{-1}. These values are two orders of magnitude larger than the residual rates measured by Parruzot et al. for the same glass at 90 °C and pH 9.3 (Parruzot et al., 2015). Assuming that diffusion of aqueous species through the growing precipitated layer has a negligible effect in these conditions, the only mechanisms that could explain this difference in kinetics between pH 7 and pH 9.3 are glass dissolution and secondary phase precipitation.

4.2. Interpretation of ToF-SIMS profiles

TEM analyses revealed that, in the tested conditions, both a smectite-type phase and amorphous silica precipitated on the glass surface. ToF-SIMS data are more complicated to explain. Here we discuss how it is possible to make them consistent with TEM data.

First, the abrasion rate of the secondary phases by the ToF-SIMS ion beam was compared with the mean abrasion rates of altered and pristine glass. Differences between these abrasions rates would lead to different depths being analyzed by ToF-SIMS for each layer. Two profiles were measured in a sample altered for 600 days, one of which was halted in the secondary phase region while the other measurement was continued into the unaltered region. The depth of the craters produced in the material was then measured by profilometry. The abrasion rate calculated using these two analyses was found to be approximately 0.03 ± 0.01 nm s^{-1} in both cases. Since the abrasion rates of the different layers are similar and assuming that the nature of the secondary phases does not change over time, this result indicates that the linear variation of the position of the Na-sharp interface given by the number of abrasion cycles (inset Fig. 5) could be used as an additional argument

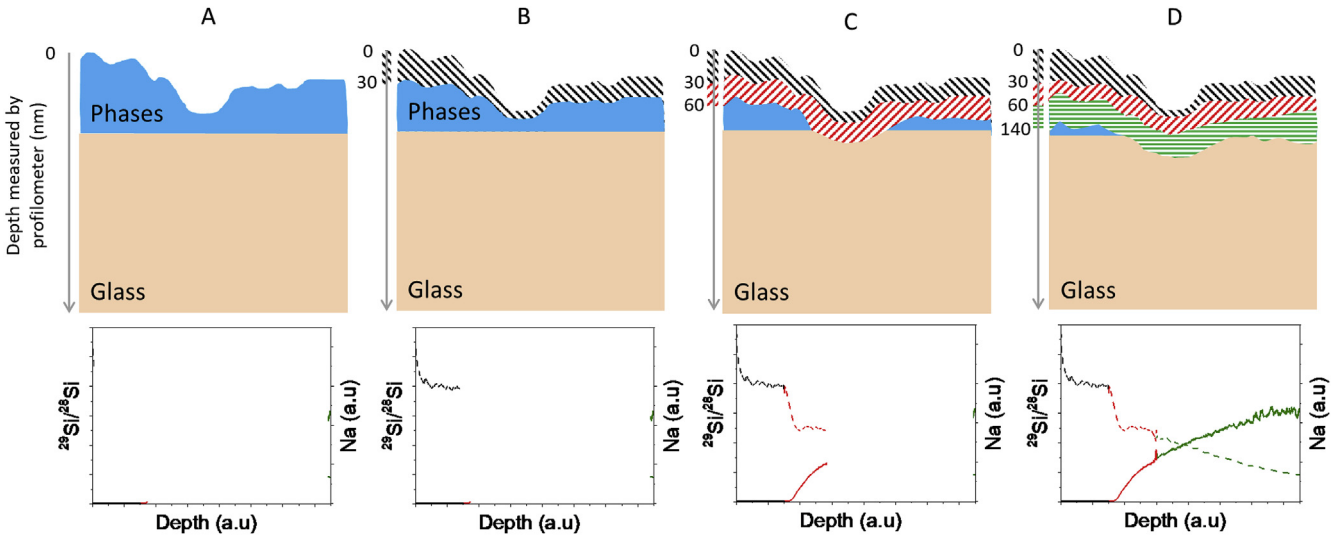

Fig. 9. *Schematic diagrams of the area analyzed by ToF-SIMS and the depth measured by profilometry (left axis) for a sample covered by an uneven layer of secondary phases.* A: initial state of the sample before analysis. The graph beneath the diagram shows the number of sodium (right axis) and silicon ($^{29}Si/^{28}Si$ isotopic ratio, left axis) counts detected. B: analysis of the first few nanometers of the precipitated phases (black line). The $^{29}Si/^{28}Si$ ratio is constant and there are close to zero Na counts. C: as the analysis proceeds (the analyzed area is shown in red), the initial roughness means that some pristine glass is measured at the same time as the secondary phases: this is a mixing region. The $^{29}Si/^{28}Si$ ratio decreases (because the silicon in the glass is at natural abundance, with $^{29}Si/^{28}Si = 0.05$) and the number of Na counts increases. D: the mixing area analyzed (in green) still contains secondary phases, but more and more pristine glass: the Na and $^{29}Si/^{28}Si$ profiles gradually reach the levels measured for pristine glass. The planar interface between the secondary phases and the glass, which should appear as a sharp step in the ToF-SIMS profile, appears instead as a gradient. (For interpretation of the references to colour in this figure legend, the reader is referred to the Web version of this article.)

in favor of a constant dissolution rate of our synthetic basaltic glass in the tested conditions.

The alteration of the glass by hydrolysis should lead to the appearance of a clear interface progressing parallel to the initial surface. However, gradients are observed in all the ToF-SIMS profiles, which seems to contradict the fact that no diffusive phenomenon was detected.

To address this issue, let us consider the behavior of Si. While the concentrations of all the elements apart from silicon plateau at the level corresponding to pristine glass at around 1200 cycles, the $^{29}Si/^{28}Si$ isotope ratio remains much higher than in the glass ($^{29}Si/^{28}Si \sim 1$, whereas at natural abundance, the ratio is 0.05). The solution cannot diffuse into the pristine glass without any rupture of the covalent bonds and thus without any release of network forming and modifying species. The high isotopic ratio is therefore not due to the entry of the solution into the glass, but to the mixing of the different regions during the analysis, as illustrated in Fig. 9. It is therefore an artifact caused by the high external roughness (from the presence of precipitates) of the samples. These mixing effects artificially enlarge the alteration front.

This artifact also makes it impossible to precisely locate the reactive region observed by TEM and thus investigate the possible diffusion release of boron and alkali elements in this region.

Time-of-flight SIMS thus only reveals the relative position of the region in which the different phases mix (i.e. they are analyzed simultaneously). Entry into this region is highlighted by a decrease in the $^{29}Si/^{28}Si$ ratio and an increase in the sodium signal.

While the shape of the gradient can be attributed to the presence of mixing areas during the analysis, the rate at which the mixing area progresses does not depend on the square root of time. The position of the front, determined from the number of abrasion/analysis cycles required to reach half the profile height, seems to advance at a constant rate (Fig. 6 inset, $R^2 = 0.87$). This comparison is valid because the different samples were analyzed under the same conditions.

Once discarded the artefacts, the ToF-SIMS data fit with the hypothesis that the glass undergoes congruent dissolution and precipitation of secondary phases.

4.3. Process governing the alteration of BG_B glass in a solution initially close to saturation with respect to amorphous silica

The results discussed above allow us to propose a reaction mechanism whereby the basaltic glass dissolves congruently in spite of the initial solution's silicon saturation.

Hydration, interdiffusion and hydrolysis of the silicate network may dominate at the very start of the alteration process. These reactions slow down very rapidly though and the silicon concentrations level out, as shown by the short-term test performed at 20000 m^{-1} (appendix 1). The interface layer of a few nanometers observed by TEM may correspond to this interface region depleted in B, Na, Ca, Fe, Ti and Mg. The most soluble elements such as B and Na accumulate in the solution, whereas the other released elements, Fe, Ti, Mg and some of the Al and Si, which are poorly soluble, precipitate, forming the secondary phases we identified. The nucleation and growth of these phases containing the main network forming species in basaltic glass may be facilitated by the presence of nickel in the solution (from the alkaline fusion reaction) and its high alkaline content. Nickel is a transition metal known to integrate into phyllosilicates and increase glass alteration (Aréna, 2016), while K, Na et Ca ensure charge balance in the clays.

Fig. 10 summarizes the mechanism we propose to explain how the basaltic glass is altered under silicon saturation conditions. Alteration is mainly driven by the precipitation of clays, which consume Si and other elements from the glass such as Mg, Fe, Al and possibly Ti. The release of these elements makes the remnant material easier to dissolve, and the additional influx of silica leads to the precipitation of amorphous silica on the surface of the glass. The glass dissolution process appears congruent overall, which means that the inward transport of water molecules or the outward transport of dissolved glass cations is not rate-limiting.

The preferential dissolution of the network modifiers increases further depolymerization of the silicate network (Devreux and Barboux, 2001; Devreux et al., 2001; Oelkers, 2001). The release of these elements leaves most of the Si atoms in Q^2 units, more hydrolysable than Q^3 and Q^4 units (the superscript in the Q^n notation indicates the number of bridging oxygens per SiO_4 tetrahedron). Once dissolved Si

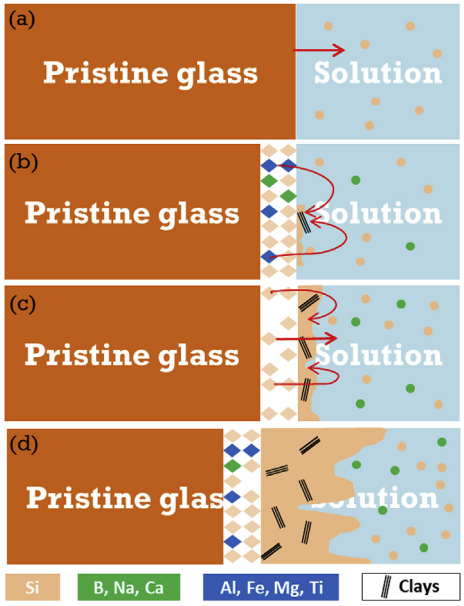

Fig. 10. Alteration process for basaltic glass under silicon saturation conditions.
a) Interdiffusion and hydrolysis lead to the release of the components of the glass; the solution rapidly becomes oversaturated with respect to clays. These phases precipitate.
b) The continued precipitation of clay minerals sustains the release of Fe, Mg, Ti and some of the Al.
c) The glass network becomes depleted in the elements composing the clays and thus highly depolymerized; it dissolves and amorphous silica precipitates.
d) The layer of secondary phases (SiO_2 + clays) becomes thicker, and so long as it does not block diffusion, the glass dissolves at a constant rate.

condense to form a gel or precipitate as amorphous silica, highly polymerized, and thermodynamically more stable structures forms.

4.4. Comparison with nuclear glass

The mechanisms governing the alteration of silicate glasses in contact with water remain a topic of interest. A particular subject of debate is the mechanism responsible for the formation of a passivating amorphous layer (Geisler et al., 2015; Gin et al., 2016, 2017; Hellmann et al., 2015; Putnis, 2015). Because basaltic glasses is considered to be a natural analogue to nuclear borosilicate glasses, the results obtained in this study contribute to re-evaluate this assertion.

Under the same experimental conditions (90 °C, pH 7, silicon-saturated solution), ISG behaves differently from BG_B (Gin et al., 2015a). The initial alteration rate of ISG ($\sim 1\,g\,m^{-2}\,d^{-1}$) decreases rapidly down to $\sim 2 \times 10^{-4}\,g\,m^{-2}\,d^{-1}$ after 365 days and then remains stable. This residual rate is 20 times lower than that measured for the basaltic glass in similar conditions. But because basaltic glass dissolves slower in the early stage of reaction (see explanation below), after one year, the equivalent thickness of altered glass is about 1.5 µm for ISG, compared with ~500 nm for BG_B. Monoliths of ISG characterized after one year of alteration show that the poorly soluble cations that make up the glass network (Si, Al and Zr) are not completely hydrolyzed during the alteration, whereas the more mobile elements (B, Na and Ca) are. The layer left behind by the release of these elements reorganizes through condensation reactions (formation of siloxane bonds) and acts as a "molecular sieve" that only lets the smallest molecules pass.

A different behavior is observed for BG_B, in which all the elements are hydrolyzed and enter the solution, before the less soluble elements precipitate in the form of secondary phases. The differences in the thickness of the altered layer and the alteration mechanism for ISG and BG_B can be explained by their different compositions. Network modifiers tend to form channels in the glass network, which facilitate the transport of cations and water therein (Greaves, 1990). The lower network modifier content of BG_B glass explains why the apparent water diffusion coefficient in the pristine glass (measured over short time periods at 50 °C and pH 3 to prevent too much hydrolysis) is higher in ISG ($9.8 \times 10^{-20}\,m^2\,s^{-1}$) than in BG_B ($5.3 \times 10^{-21}\,m^2\,s^{-1}$) (Parruzot et al., 2015). This also explains the better chemical durability of BG_B under initial rate conditions. The initial dissolution rate of BG_B is indeed $0.15 \pm 0.07\,g\,m^{-2}\,d^{-1}$ at 90 °C and pH 7 (Parruzot, 2014), compared with $1.2\,g\,m^{-2}\,d^{-1}$ for ISG under the same conditions (Inagaki et al., 2013).

Although experimental data showed that, under silica saturated solution and near neutral pH, basaltic glass behaves according to the interfacial dissolution/precipitation mechanism whereas ISG alteration leaves a leached-and-reorganized layer which progressively passivates the glass surface, the origin of this difference remains to be discussed.

Despite the same molar ratios, ISG differs from CJ1 glass (Table 1) in that the former contains "hardening" elements such as Zr and Al (six-fold and 4-fold coordinated elements with energy barriers for hydrolysis at neutral and basic pHs higher than for Si-O-Si). The effect of these elements is so strong that the silicate network of ISG does not dissolve in a solution close to saturation with respect to amorphous silica (Gin et al., 2018; Gin et al., 2015a), whereas CJ1 glass does (Jegou et al., 2000). Zr is known to prevent both silicate network hydrolysis and gel reorganization and lowers the concentration of dissolved silica at saturation (Cailleteau et al., 2008; Cailleteau et al., 2011). Moreover, until 90 °C no secondary phases involving Si and Zr can precipitate at the expense of the gel. As a consequence, the presence of Zr in ISG might explain why passivating gels formed by leaching and reorganization. Aluminum is known to be strongly retained in the gel (Chave, 2008; Noguès, 1984), because of its low solubility at neutral and alkaline pHs. To a lower extent relative to Zr (because of its lower coordination number), Al can also act as a cross-linking element in the gel and thus contributes to its passivating nature. But, in the presence of Mg or some transition metals Al contributes to the precipitation of phyllosilicates (Aréna et al., 2017; Arena et al., 2016; Curti et al., 2006), or under hyper alkaline pH to the precipitation of calcium silicate hydrates or zeolites (Fournier et al., 2014a; Fournier et al., 2017; Gin et al., 2015b; Piovesan et al., 2018). By consuming Si, these minerals form at the expense of the gel. Finally, Ca, which is present in ISG but not in CJ1 glass, also has a strong effect on the passivation properties of the gel layer (Chave et al., 2011; Mercado-Depierre et al., 2013; Rebiscoul et al., 2012). The presence of both Ca and Zr in glass leads to the formation very efficient passivating layers (Gin et al., 2012).

With BG_B it is shown that when aluminum is destabilized and enters secondary phases, it loses its crosslinking effect in the gel. The good chemical durability of ISG with respect to hydrolysis therefore seems to stem from the fact that this glass does not contain any elements liable to form secondary crystalline phases (under the experimental conditions used in this study, namely 90 °C and a near neutral pH). Contrary to what happens in BG_B therefore, the network of glass-forming species remains unperturbed and can reorganize into a dense and passivating gel following the release of the more mobile elements.

5. Conclusion

Basaltic glass is commonly considered as a natural analogue of nuclear glasses. To re-examine this assertion, a key experiment designed to study the formation mechanisms of the passivating layer on ISG (Gin et al., 2015a) was repeated for the sake of comparison using a synthetic basaltic glass. In our experiments, beyond the reaction interface layer, a few nanometers thick, no passivating or other material similar to the alteration gel observed on nuclear glass formed.

The size and properties of the reactive area are difficult to determine using this experiment. Alteration probably starts with the preferential release of alkaline species from the glass, but this must only affect a few

nanometers. This process depolymerizes the glass and makes the network-forming species involved in secondary phases more hydrolysable. This transfer of elements to secondary phases is the main driver of alteration, destabilizing the silicate network in spite of the high concentration of dissolved silica in the solution.

Overall, this study highlights the strong effect of glass composition on the mechanism that limits the alteration rate of the glass in the long term. For basaltic glasses, the main mechanism under the tested conditions is the interfacial dissolution-precipitation reaction. For ISG, alteration is controlled by the formation of a passivating layer by in situ reorganization of the silicate network after the preferential leaching of weakly bonded species.

Acknowledgements

This research was funded by the following organizations: CEA, IPGP and IRSN.

ANNEX

Annex 1: Short term tests

Given that the S/V ratio does not alter the release rate of mobile species under these experimental conditions (Gin et al., 2013b) a higher S/V ratio (20000 m^{-1}) was used in a short term test to explore the initial stages of alteration under saturation conditions. The evolution of the solution is shown in Table A1 and Fig. A1, with a reduction in the B-measured alteration rate of nearly 2 orders of magnitude over the first 7 days. At the same time, the pH remains stable and the concentration of silica increases slightly. The decrease in the amount of boron released seems to be proportional to the square root of time, a behavior that is generally associated with diffusion controlled phenomena. This short time test with a higher S/V ratio clearly shows that the glass starts to become altered very rapidly.

Table A1
Data from solution analyses for 20000m^{-1} test.

t	$pH_{90°C}$	Si_{tot}	B	ETh(B)	Rate
(days)		($mg.L^{-1}$)	($mg.L^{-1}$)	nm	($g.m^{-2}.d^{-1}$)
0	7.0	160.0	< 0.3	–	–
0.06	7.2	160.9	0.50	3.1	0.152
0.09	7.1	170.2	0.51	3.1	0.101
0.17	7.1	167.6	0.69	4.1	0.066
0.33	7.2	182.5	0.84	5.0	0.042
1.01	7.0	173.0	1.10	6.4	0.018
1.99	7.0	168.9	1.17	6.7	0.009
7.01	7.1	171.1	1.32	7.5	0.003

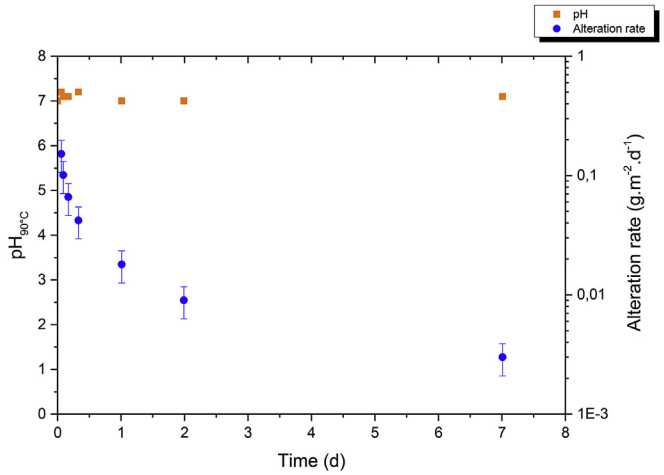

Fig. A1. *Glass dissolution rate from [B] (●, right axis) and* $pH_{90°C}$ *(■, left axis) in the* 20000m^{-1} *test.*

The initial rate decreases rapidly toward 3.10^{-3} $g\,m^{-2}\,d^{-1}$ after 7 days, which is similar to the long-term values measured in the main experiment, namely between 1.9 et 4.4 10^{-3} $g\,m^{-2}\,d^{-1}$ depending on the tracer used.

During this stationary stage, the layer of altered glass is roughly 5 nm thick. This is of the same order or magnitude as the thickness of the interface layer observed by TEM in the main experiment.

References

Aréna, H., 2016. Effets cumulatifs et compétitifs des éléments chimiques sur l'altération des verres nucléaires. Thèse de l'Université Montpellier 2. .

Aréna, H., et al., 2017. Impact of iron and magnesium on glass alteration: characterization of the secondary phases and determination of their solubility constants. Appl. Geochem. 82 (Suppl. C), 119–133.

Arena, H., et al., 2016. Impact of Zn, Mg, Ni and Co elements on glass alteration: additive effects. J. Nucl. Mater. 470, 55–67.

Barone, G., et al., 2016. Nanoscale surface modification of Mt. Etna volcanic ashes. Geochem. Cosmochim. Acta 174, 70–84.

Benzerara, K., et al., 2007. Alteration of submarine basaltic glass from the Ontong Java Plateau: a STXM and TEM study. Earth Planet Sci. Lett. 260 (1–2), 187–200.
Berger, G., Schott, J., Loubet, M., 1987. Fundamental processes controlling the 1st stage of aleration of a basalti glass by seawater - an experimental-study between 200-degrees-C ans 320-degrees-C. Earth Planet Sci. Lett. 84 (4), 431–445.
Brunauer, S., Emmett, P.H., Teller, E., 1938. Adsorption of gases in multimolecular layers. J. Am. Chem. Soc. 60 (2), 309–319.
Bunker, B.C., 1994. Molecular mechanisms for corrosion of silica and silicate-glasses. J. Non-Cryst. Solids 179, 300–308.
Cailleteau, C., et al., 2008. Insight into silicate-glass corrosion mechanisms. Nat. Mater. 7 (12), 978–983.
Cailleteau, C., Devreux, F., Spalla, O., Angeli, F., Gin, S., 2011. Why do certain glasses with a high dissolution rate undergo a low degree of corrosion? J. Phys. Chem. C 115 (13), 5846–5855.
Chave, T., 2008. Etude des mécanismes d'altéraion par l'eau du verre R7T7 en milieu confiné, compréhension et modélisation de la cinétique résiduelle. Thèse de l'Université Montpellier 2, Sciences et Techniques du Languedoc. .
Chave, T., Frugier, P., Gin, S., Ayral, A., 2011. Glass-water interphase reactivity with calcium rich solutions. Geochem. Cosmochim. Acta 75 (15), 4125–4139.
Collin, M., Fournier, M., Charpentier, T., Moskura, M., Gin, S., 2018. Impact of alkali on the passivation of silicate glass. npj-Materials Degradation 2, 16.
Crovisier, J.L., 1989. Dissolution des verres basaltiques dans l'eau de mer et dans l'eau douce. Essai de modélisation. Doctorat Thesis. Université Louis Pasteur (Strasbourg), pp. 251.
Crovisier, J.L., Advocat, T., Dussossoy, J.L., 2003. Nature and role of natural alteration gels formed on the surface of ancient volcanic glasses (Natural analogs of waste containment glasses). J. Nucl. Mater. 321, 91–109.
Crovisier, J.L., Honnorez, J., Eberhart, J.P., 1987. Dissolution of basaltic glass in seawater: mechanism and rate. Geochem. Cosmochim. Acta 51, 2977–2990.
Curti, E., Crovisier, J.L., Morvan, G., Karpoff, A.M., 2006. Long-term corrosion of two nuclear waste reference glasses (MW and SON68): a kinetic and mineral alteration study. Appl. Geochem. 21 (7), 1152–1168.
Daux, V., Guy, C., Advocat, T., Crovisier, J.L., Stille, P., 1997. Kinetic aspects of basaltic glass dissolution at 90 degrees C: role of aqueous silicon and aluminium. Chem. Geol. 142 (1–2), 109–126.
Devreux, F., Barboux, P., 2001. Numerical modelling of glass dissolution : gel layer morphology. J. Nucl. Mater. 298 (1,2), 145–149.
Devreux, F., Barboux, P., Filoche, M., Sapoval, B., 2001. A simplified model for glass dissolution in water. J. Mater. Sci. 36, 1331–1341.
Ewing, R.C., 1979. Natural Glasses: Analogues for Radioactive Waste forms., Scientific Basis for Nuclear Waste Management I. Materials Research Society, Boston, pp. 57–66.
Fournier, M., Frugier, P., Gin, S., 2014a. Resumption of alteration at high temperature and pH: rates measurements and comparison with initial rates. In: 2nd International Summer School on Nuclear Glass Wasteform: Structure, Properties and Long-Term Behavior (Sumglass 2013), 7: 202–208.
Fournier, M., Gin, S., Frugier, P., 2014b. Resumption of nuclear glass alteration: state of the art. J. Nucl. Mater. 448 (1–3), 348–363.
Fournier, M., Gin, S., Frugier, P., Mercado-Depierre, S., 2017. Contribution of zeolite-seeded experiments to the understanding of resumption of glass alteration. NPJ-Mater. Degrad. 1, 17.
Fournier, M., et al., 2016. Glass dissolution rate measurement and calculation revisited. J. Nucl. Mater. 476, 140–154.
Frugier, P., et al., 2008. SON68 nuclear glass dissolution kinetics: current state of knowledge and basis of the new GRAAL model. J. Nucl. Mater. 380 (1–3), 8–21.
Geisler, T., et al., 2010. Aqueous corrosion of borosilicate glass under acidic conditions: a new corrosion mechanism. J. Non-Cryst. Solids 356 (28–30), 1458–1465.
Geisler, T., et al., 2015. The mechanism of borosilicate glass corrosion revisited. Geochem. Cosmochim. Acta 158, 112–129.
Georg, R.B., Reynolds, B.C., Frank, M., Halliday, A.N., 2006. New sample preparation techniques for the determination of Si isotopic compositions using MC-ICPMS. Chem. Geol. 235 (1–2), 95–104.
Gin, S., 2014. Open scientific questions about nuclear glass corrosion. In: 2nd International Summer School on Nuclear Glass Wasteform: Structure, Properties and Long-term Behavior (Sumglass 2013), vol. 7. pp. 163–171.
Gin, S., et al., 2013a. An international initiative on long-term behavior of high-level nuclear waste glass. Mater. Today 16 (6), 243–248.
Gin, S., Beaudoux, X., Angeli, F., Jegou, C., Godon, N., 2012. Effect of composition on the short-term and long-term dissolution rates of ten glasses of increasing complexity from 3 to 30 oxides. J. Non-Cryst. Solids 358 (18–19), 2559–2570.
Gin, S., et al., 2018. Dynamics of self-reorganization explains passivation of silicate glasses. Nat. Commun. 9.
Gin, S., Frugier, P., Jollivet, P., Bruguier, F., Curti, E., 2013b. New insight into the residual rate of borosilicate glasses: effect of S/V and glass composition. International Journal of Applied Glass Science 4 (4), 371–382 submitted to.
Gin, S., et al., 2017. Atom-Probe Tomography, TEM and ToF-SIMS study of borosilicate glass alteration rim: a multiscale approach to investigating rate-limiting mechanisms. Geochem. Cosmochim. Acta 202 (Suppl. C), 57–76.
Gin, S., et al., 2015a. Origin and consequences of silicate glass passivation by surface layers. Nat. Commun. 6.
Gin, S., et al., 2015b. The fate of silicon during glass corrosion under alkaline conditions: a mechanistic and kinetic study with the International Simple Glass. Geochem. Cosmochim. Acta 151, 68–85.
Gin, S., et al., 2016. The controversial role of inter-diffusion in glass alteration. Chem. Geol. 440, 115–123.
Gislason, R., Eugster, H.P., 1987. Meteoric water-basalt interactions. I: a laboratory study. Geochem. Cosmochim. Acta 51, 2827–2840.
Gislason, S.R., Oelkers, E.H., 2003. Mechanism, rates, and consequences of basaltic glass dissolution: II. An experimental study of the dissolution rates of basaltic glass as a function of pH and temperature. Geochem. Cosmochim. Acta 67 (20), 3817–3832.
Gislason, S.R., et al., 2013. Solubility and mineral storage of CO_2 in basalt. Mineral. Mag. 77 (5), 1178.
Gourgiotis, A., et al., 2017. Silicon isotope ratio measurements by inductively coupled plasma tandem mass spectrometry for alteration studies of nuclear waste glasses. Anal. Chim. Acta 954 (Suppl. C), 68–76.
Grambow, B., Muller, R., 2001. First-order dissolution rate law and the role of surface layers in glass performance assessment. J. Nucl. Mater. 298 (1–2), 112–124.
Greaves, G.N., 1990. EXAFS for studying corrosion of glass surfaces. J. Non-Cryst. Solids 120, 108–116.
Guyot, F., et al., 2011. CO_2 geological storage: the environmental mineralogy perspective. Compt. Rendus Geosci. 343 (2), 246–259.
Hellmann, R., et al., 2015. Nanometre-scale evidence for interfacial dissolution-re-precipitation control of silicate glass corrosion. Nat. Mater. 14 (3), 307–311.
Icenhower, J.P., Steefel, C.I., 2015. Dissolution rate of borosilicate glass SON68: a method of quantification based upon interferometry and implications for experimental and natural weathering rates of glass. Geochem. Cosmochim. Acta 157, 147–163.
Inagaki, K., Furuya, H., Idemitsu, K., Arima, T., 1998. Review of waste glass corrosion and associated radionuclide release as a part of safety assessment of entire disposal system. Prog. Nucl. Energy 32 (3–4), 501–508.
Inagaki, Y., Kikunaga, T., Idemitsu, K., Arima, T., 2013. Initial dissolution rate of the international simple glass as a function of pH and temperature measured using microchannel flow-through test method. Int. J. Appl. Glass Sci. 4 (4), 317–327.
Jantzen, C.M., Brown, K.G., Pickett, J.B., 2010. Durable glass for thousands of years. Int. J. Appl. Glass Sci. 1 (1), 38–62.
Jegou, C., Gin, S., Larche, F., 2000. Alteration kinetics of a simplified nuclear glass in an aqueous medium: effects of solution chemistry and of protective gel properties on diminishing the alteration rate. J. Nucl. Mater. 280 (2), 216–229.
Jégou, C., Gin, S., Larché, F., 2000. Alteration kinetics of a simplified nuclear glass in an aqueous medium: effects of solution chemistry and of protective gel properties on diminishing the alteration rate. J. Nucl. Mater. 280 (2), 216–229.
Jercinovic, M.J., Keil, K., Smith, M.R., Schmitt, R.A., 1990. Alteration of basaltic glasses from north-central British Columbia, Canada. Geochem. Cosmochim. Acta 54, 2679–2696.
Jollivet, P., et al., 2008. Investigation of gel porosity clogging during glass leaching. J. Non-Cryst. Solids 354 (45–46), 4952–4958.
Le Gal, X., 1999. Etude de l'altération de verres volcaniques du Vatnajökull (Islande). Mécanismes et bilans à basse température. Université Louis Pasteur de Strasbourg, pp. 153.
Libourel, G., et al., 2011. The use of natural and archeological analogues for understanding the long-term behavior of nuclear glasses. Compt. Rendus Geosci. 343 (2–3), 237–245.
Mercado-Depierre, S., Angeli, F., Frizon, F., Gin, S., 2013. Antagonist effects of calcium on borosilicate glass alteration. J. Nucl. Mater. 441 (1–3), 402–410.
Morin, G.P., Vigier, N., Verney-Carron, A., 2015. Enhanced dissolution of basaltic glass in brackish waters: impact on biogeochemical cycles. Earth Planet Sci. Lett. 417, 1–8.
Noguès, J.-L., 1984. Les mécanismes de corrosion des verres de confinement des produits de fission. Thèse de l'Université des Sciences et Techniques du Languedoc.
Oelkers, E.H., 2001. General kinetic description of multioxide silicate mineral and glass dissolution. Geochem. Cosmochim. Acta 65 (21), 3703–3719.
Parruzot, B., 2014. Altération des verres basaltiques dans des environnements confinés : analogie avec le stockage des verres nucléaires. Université de Montpellier.
Parruzot, B., Jollivet, P., Rebiscoul, D., Gin, S., 2015. Long-term alteration of basaltic glass: mechanisms and rates. Geochem. Cosmochim. Acta 154, 28–48.
Piovesan, V., et al., 2018. Chemical durability of peraluminous glasses for nuclear waste conditioning. NPJ-Mater. Degrad. 2, 7.
Poinssot, C., Gin, S., 2012. Long-term Behavior Science: the cornerstone approach for reliably assessing the long-term performance of nuclear waste. J. Nucl. Mater. 420 (1–3), 182–192.
Pringle, E.A., Moynier, F., Savage, P.S., Badro, J., Barrat, J.A., 2014. Silicon isotopes in angrites and volatile loss in planetesimals. Proc. Natl. Acad. Sci. U.S.A. 111 (48), 17029–17032.
Pringle, E.A., et al., 2016. Silicon isotopes reveal recycled altered oceanic crust in the mantle sources of Ocean Island Basalts. Geochem. Cosmochim. Acta 189, 282–295.
Putnis, A., 2015. Glass corrosion: sharpened interface. Nat. Mater. 14 (3), 261–262.
Rebiscoul, D., Bruguier, F., Magnin, V., Gin, S., 2012. Impact of soda-lime borosilicate glass composition on water penetration and water structure at the first time of alteration. J. Non-Cryst. Solids 358 (22), 2951–2960.
Rebiscoul, D., Frugier, P., Gin, S., Ayral, A., 2005. Protective properties and dissolution ability of the gel formed during nuclear glass alteration. J. Nucl. Mater. 342 (1–3), 26–34.
Rebiscoul, D., et al., 2004. Morphological evolution of alteration layers formed during nuclear glass alteration: new evidence of a gel as a diffusive barrier. J. Nucl. Mater. 326 (1), 9–18.
Savage, P.S., Moynier, F., 2013. Silicon isotopic variation in enstatite meteorites: clues to their origin and Earth-forming material. Earth Planet Sci. Lett. 361, 487–496.
Stockmann, G.J., Wolff-Boenisch, D., Gislason, S., Oelkers, E.H., 2011. Do carbonate precipitates affect dissolution kinetics? 1: Basaltic glass. Chem. Geol. 284 (3–4), 306–316.
Techer, I., Advocat, T., Lancelot, J., Liotard, J.,M., 2000. Basaltic glass: alteration mechanisms and analogy with nuclear waste glasses. J. Nucl. Mater. 282, 40–46.
Techer, I., Advocat, T., Lancelot, J., Liotard, J.,M., 2001. Dissolution kinetics of basaltic glasses : control by solution chemistry and protective effect of the alteration film.

Chem. Geol. 176, 235–263.
Valkiers, S., Russe, K., Taylor, P., Ding, T., Inkret, M., 2005. Silicon isotope amount ratios and molar masses for two silicon isotope reference materials: IRMM-018a and NBS28. Int. J. Mass Spectrom. 242 (2–3), 319–321.
Van Iseghem, P., et al., 2009. Glamor - or how we achieved a common understanding on the decrease of glass dissolution kinetics. Environ. Issues. Waste Manag. Technol. Mater. Nuclear Ind. XII (207), 115–121.
Van Iseghem, P., et al., 2006. Chemical durability of high-level waste glass in repository environment: main conclusions and remaining uncertainties from the GLASTAB and GLAMOR projects. Sci. Basis. Nucl. Waste Manag. XXIV (932), 293–299.
Verney-Carron, A., Vigier, N., Millot, R., 2011. Experimental determination of the role of diffusion on Li isotope fractionation during basaltic glass weathering. Geochem. Cosmochim. Acta 75 (12), 3452–3468.
Vienna, J.D., Ryan, J.V., Gin, S., Inagaki, Y., 2013. Current understanding and remaining challenges in modeling long-term degradation of borosilicate nuclear waste glasses. Int. J. Appl. Glass Sci. 4 (4), 283–294.
Wolff-Boenisch, D., Gislason, S.R., Oelkers, E.H., Putnis, C.V., 2004. The dissolution rates of natural glasses as a function of their composition at pH 4 and 10.6, and temperatures from 25 to 74 degrees C. Geochem. Cosmochim. Acta 68 (23), 4843–4858.
Wolff-Boenisch, D., Wenau, S., Gislason, S.R., Oelkers, E.H., 2011. Dissolution of basalts and peridotite in seawater, in the presence of ligands, and CO_2: implications for mineral sequestration of carbon dioxide. Geochem. Cosmochim. Acta 75 (19), 5510–5525.
Zapol, P., He, H., Kwon, K.D., Criscenti, L.J., 2013. First-principles study of hydrolysis reaction barriers in a sodium borosilicate glass. Int. J. Appl. Glass Sci. 4 (4), 395–407.